

Article

Design and Fabrication of a Narrow Bandpass Filter with Low Dependence on Angle of Incidence

Yi-Jun Jen * and Meng-Jie Lin

Department of Electro-Optical Engineering, National Taipei University of Technology, Taipei 106, Taiwan; mjlin@ntut.edu.tw

* Correspondence: jyun@ntut.edu.tw; Tel.: +886-2-2771-2171 (ext. 4626)

Received: 31 May 2018; Accepted: 27 June 2018; Published: 29 June 2018



Abstract: A multilayer narrow bandpass filter that consists of silver and silicon thin films is designed using the admittance tracing method. Owing to the low loss of silicon in the infrared range, the peak transmittance at a wavelength of 950 nm exceeds 85%. To eliminate the sidebands that are adjacent to the passband, a compact four-layered structure is proposed to generate an angle-insensitive spectrum. In fabrication, a silver-silicon multilayer is deposited to approach the design.

Keywords: interference coatings; multilayer design; spectral properties

1. Introduction

An optical bandpass filter selectively reflects or transmits specific wavelengths, and has a wide range of applications, including display, optical communications, and sensing [1–4]. Bandpass filters can be divided into two types, which are absorption filters and optical interference filters. Absorption filters that are based on organic dyes or chemical pigments operate by passing a specific range of wavelengths and attenuating light at other wavelengths; they are easily degraded by long-term ultraviolet illumination and high temperature [5]. Other filters are mostly made using optical interference coatings [6] to yield the desired bandpass spectra. Even though the interference filter has high stability and good wavelength-selectivity, most of those interference filters depend on angle of incidence because the phase thickness and equivalent admittance of each layer are both functions of angle of incidence. Over the last decade, many studies of optical coatings have been undertaken with a view to developing a bandpass filter with an angle-independent spectrum. Most such efforts have combined metal and dielectric films to form a multilayer to generate colors that are insensitive to angles of incidence (AOI). In 2015, a multilayer angle-insensitive color filter that was composed of Si, Ag, Cr, and TiO₂ films was fabricated with a passband over 200 nm and a variation of transmittance of approximately 20% over AOI from 0° to 50° [7].

Recently, plasmonic nanostructures, including nanorods [8] and nanocavities [9], with filtering capability have been proposed. However, the angle-insensitivity of plasmonic nanostructured filters has always been achieved by sacrificing the output light intensity. For example, the angle-insensitivity of a silver cross-shaped nanohole array can be maintained up to 35° for both polarizations in the near-infrared region, but the transmittance of the passband is less than 50% [10]. In a previous work, a one-dimensional grating structure has been used as a wide-angle bandpass filter but only for one polarization [11]. Although extensive efforts are being made to generate structural colors in an angle-independent manner, an angle-independent filter with high transmission and a passband with a narrow bandwidth is still sought.

In our previous work, a modified Fabry–Perot filter was developed on a normalized admittance diagram (NAD) [12]. The normalized admittance tracing method is adopted herein to design a narrow-passband filter. Any multilayer on a substrate is equivalent to a medium with an admittance

of η_{eq} adjacent to the incident medium with a refractive index of N_i . Therefore, the reflection coefficient can be obtained using the familiar equation $r = (N_i - \eta_{eq}) / (N_i + \eta_{eq})$. At oblique incidence, the admittance is further normalized to $\eta_p = N \cos \theta_i / \cos \theta$ for p-polarization and $\eta_s = N \cos \theta / \cos \theta_i$ for s-polarization, where θ_i and θ are the angle of refraction in the medium and the AOI in the incident medium, respectively. As films are grown on a substrate, the resulting variation of equivalent admittance can be simulated by tracing the equivalent admittance in the complex plane.

Admittance matching was exploited to design an $N_i / M_1 D_2 M_3 D_4 \dots M_{i-2} D_{i-1} M_i / N_{sub}$ system of alternatively arranged metal and dielectric thin films, where N_i and N_{sub} are the incident medium and the substrate; and M and D denote the metal and dielectric films, respectively. The design was developed on the NAD by using metal films (M_3, M_5, \dots, M_{i-2}) between the top and bottom metals (M_1 and M_i) to generate large loci that reduces the dissipation of light within the middle metal films. Using metal and dielectric films of silver and silicon, respectively, causes the multilayer to exhibit a negative index of refraction when the fraction of metal is high enough to support the localized magnetic resonance. Although the design induces transmission, the extinction properties of both Ag and Si keep the transmittance below 18% at a wavelength of 670 nm. However, this passband is angle-insensitive. Since Ag has a smaller index of refraction and Si has a larger index of refraction than that of the incident medium of air, the variation of the angle of refraction in the films with the AOI is small, maintaining constant phase thickness and admittances of η_p and η_s over a wide range of AOI. An angle-insensitive filter with a symmetrical passband and optimum transmission based on the combination of a modified Fabry–Perot filter and extreme refraction indices is sought. In this work, a bandpass filter that is angle-insensitive at a wavelength $\lambda_0 = 950$ nm is developed, at which the extinction coefficient of Si is lower than 0.002. The loss of the metal-dielectric filter arises from the metal films. This design also eliminates the sidebands that often exist adjacent to the designate passband. To our knowledge, this work owns the originality to consider those factors including narrowband, high transmission, angular insensitivity, and sideband elimination together. Although modern design programs have been developed, a comprehensive method is still necessary to offer an initial configuration for optimum calculation.

2. Methods

Figure 1a plots the normalized admittance loci of a five-layered Fabry–Perot design $N_i / M_1 D_2 M_3 D_4 M_5 / N_{sub}$. The bottom D_4 and M_5 cause the equivalent admittance to be a complex value $N = n + ik$ with large positive k and small n , causing the locus of M_3 to be a large contour. To form an angle-insensitive filter, the metal and dielectric films were made of silver and silicon, respectively. For smaller index of extinction coefficient, the semiconductor of a-Si was used as a dielectric in near-infrared region. The refractive indexes of Ag and a-Si were taken from the database in the Macleod thin-film package [6], and the dispersion of metal and dielectric films was taken into account. The refractive indexes as functions of wavelength are shown in Appendix A. The filter was designed to pass a wavelength of 950 nm. The thicknesses of M_5 and D_4 were 20 nm and 97 nm, respectively, causing the terminal normalized admittance (NA) to be at (14.003, 19.189). The thickness of M_3 was set to 10 nm, which is feasible for an ultra-thin silver film that was formed by e-beam evaporation or sputtering evaporation. The top two layers M_1 and D_2 functioned as matching layers to bring the equivalent admittance back to the admittance of the incident medium. Therefore, the designed five-layered Fabry–Perot filter became $N_i / M_1 D_2 M_3 D_4 M_5 / N_{sub} = \text{air} / \text{Ag}(13 \text{ nm}) / \text{a-Si}(90 \text{ nm}) / \text{Ag}(10 \text{ nm}) / \text{a-Si}(97 \text{ nm}) / \text{Ag}(20 \text{ nm}) / \text{BK7 glass}$. The associated transmittance spectrum of the five-layered system in Figure 1b indicated that the passband was not a symmetrical peak and sideband occurred on one side of the design wavelength. Figure 1c shows the NA diagram at the central wavelength of a sideband, 1326 nm. Although the wavelength was longer (shorter) than the design wavelength, all loci were shortened (lengthened), but the terminal point remains around unity on the real axis. The compensation was caused by the top two layers M_1 and D_2 . The shrinkage or expansion of loci M_1 and D_2 kept the admittance of the

terminal close to that of the incident medium. For the five-layered Fabry–Perot design, the oxidation of metal film on the top would affect the performance of the filter. Although a low-index, thin film with half-wave thickness can be coated on the top of a metal film to function as a protective layer, the performance of filtering only maintains at normal incidence. At oblique incidence, the bandpass spectrum is affected due to the angular dependent admittance and phase thickness of the protective layer. Therefore, it was desired to modify the design to have dielectric layer on the top to support the avoidance of oxidation.

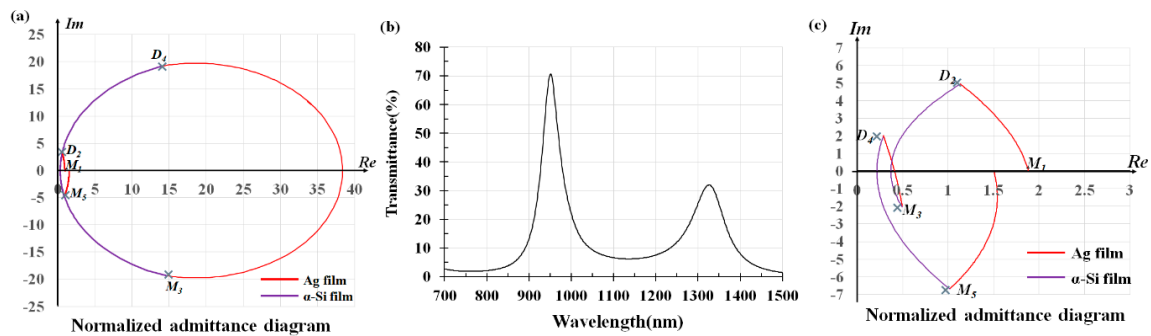


Figure 1. (a) Normalized admittance diagram (NAD) loci of modified five-layered filter with structure $N_i/M_1D_2M_3D_4M_5/N_{sub}$; (b) transmittance spectrum of five-layered system; (c) NAD loci at a wavelength of 1326 nm.

To eliminate the sideband effect and to increase the sensitivity to wavelength, the multilayer system was changed to a four-layered $N_i/D_1M_2D_3M_4/N_{sub} = \text{air}/\text{a-Si}(67 \text{ nm})/\text{Ag}(15 \text{ nm})/\text{a-Si}(84 \text{ nm})/\text{Ag}(16 \text{ nm})/\text{BK7 glass}$ system. The sideband comes from the admittance matching that occurs at another wavelength in the five-layered system. A four-layered system proposed here can avoid the unnecessary admittance matching. The loci of M_2 and D_1 are sensitive to the variation of wavelength to lead to a narrow passband. Figure 2a shows the designed loci of a passband filter. After the large locus of M_2 , the locus of D_1 directly brings the admittance of the terminal back to that of the incident medium. This design yields the spectrum that is shown in Figure 2b. The maximum transmittance at a wavelength of 950 nm is 85% and the full width at half maximum (FWHM) of the passband is 117 nm. In the wavelength range from 700 nm to 1500 nm, the only transmission peak was the designed one. To increase the resolution of the bandpass filter, the four-layered design was modified to reduce the FWHM. The thickness of D_3 was increased from 84 nm to 212 nm to take one more loop of locus in NAD. The large phase thickness of D_3 varies markedly with wavelength. As shown in Figure 3, the maximum transmittance of the four-layered $N_i/D_1M_2D_3M_4/N_{sub} = \text{air}/\text{a-Si}(67 \text{ nm})/\text{Ag}(15 \text{ nm})/\text{a-Si}(212 \text{ nm})/\text{Ag}(16 \text{ nm})/\text{BK7 glass}$ at a wavelength of 950 nm is 85% and the FWHM of the passband is 83 nm.

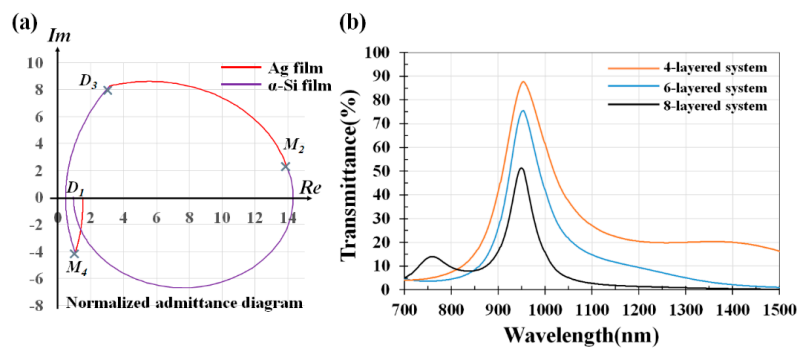


Figure 2. (a) NAD loci and (b) transmittance spectra of four-layered $N_i/D_1M_2D_3M_4/N_{sub} = \text{air/a-Si (67 nm)/Ag(15 nm)/a-Si(84 nm)/Ag(16 nm)/glass}$, six-layered $N_i/D_1M_2D_3M_4D_5M_6/N_{sub} = \text{air/a-Si(52 nm)/Ag(11 nm)/a-Si(40 nm)/Ag(13 nm)/a-Si(75 nm)/Ag(20 nm)/BK7 glass}$ system, and eight-layered $N_i/D_1M_2D_3M_4D_5M_6D_7M_8/N_{sub} = \text{air/a-Si(60 nm)/Ag(13 nm)/a-Si(50 nm)/Ag(11 nm)/a-Si(53 nm)/Ag(13 nm)/a-Si(50 nm)/Ag(20 nm)/BK7 glass}$ system.

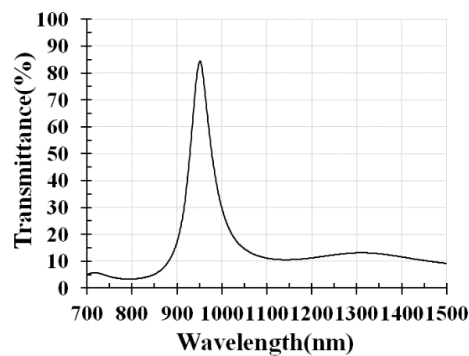


Figure 3. Transmittance spectrum of $N_i/D_1M_2D_3M_4/N_{sub} = \text{air/a-Si(67 nm)/Ag(15 nm)/a-Si(212 nm)/Ag(16 nm)/BK7 glass}$.

The admittance matching design can be extended to six-layered and eight-layered structures as $N_i/D_1M_2D_3M_4D_5M_6/N_{sub} = \text{air/a-Si(52 nm)/Ag(11 nm)/a-Si(40 nm)/Ag(13 nm)/a-Si(75 nm)/Ag(20 nm)/BK7 glass}$ system and $N_i/D_1M_2D_3M_4D_5M_6D_7M_8/N_{sub} = \text{air/a-Si(60 nm)/Ag(13 nm)/a-Si(50 nm)/Ag(11 nm)/a-Si(53 nm)/Ag(13 nm)/a-Si(50 nm)/Ag(20 nm)/BK7 glass}$ system, respectively. The corresponding spectra are shown in Figure 2b. The transmittance decreases with increasing number of layers. In the case of eight-layered structure, although the transmittance at wavelengths over 1050 nm is suppressed to be less than 4.7%, the peak transmittance is also reduced to be 50%.

3. Experiments and Results

An experiment was performed to fabricate a four-layered filter with the specified design. Firstly, a single layer of silver and a single layer of a-Si were deposited by sputtering. The Ag layers were fabricated using a radio-frequency (RF) magnetron sputtering method. The Ag target with a diameter of 3 in, a thickness of 4 mm and a purity of 99.99%, attached to a Cu plate, was used for sputtering. The a-Si layers were fabricated using a direct current (DC) sputtering method. Then, the a-Si target with a diameter of 3.5 in, a thickness of 4 mm, and a purity of 99.99%, attached to a Cu plate, was used for sputtering. The temperature of substrate during the a-Si deposition and Ag deposition was controlled at 25 °C. Before the multilayer deposition, a uniform silver film with a thickness of 10 nm was deposited on a glass substrate. The refractive index of deposited silver film was measured and compared with the database of Macleod package, as shown in Figures A1 and A2. The consistence between both

measured refractive and the database concludes that the silver film is homogeneous. The refractive indexes of a-Si as functions of wavelength are shown in Figures A3 and A4. The refractive indexes of silver and a-Si were obtained as functions of wavelength from measured spectra of the ellipsometric parameters and transmittance. The refractive indexes of Ag and a-Si at the wavelength of 950 nm were measured to be $0.31 + 6.83i$ and $3.85 + 0.06i$, respectively. Based on the refractive indexes of Ag and a-Si, the measured optical constants were used to re-design the filter as $N_i/D_1M_2D_3M_4/N_{sub} = \text{air/a-Si (57 nm)/Ag (20 nm)/a-Si (88 nm)/Ag (20 nm)/BK7 glass}$. Figure 4 shows a cross-sectional SEM image, which shows the thickness of each layer in $N_i/D_1M_2D_3M_4/N_{sub} = \text{air/a-Si (55 nm)/Ag (20 nm)/a-Si (87 nm)/Ag (20 nm)/BK7 glass}$. There is indeed an oxide layer with thickness of 3 nm above the top a-Si layer. Based on previous investigations [13,14], the surface of the a-Si layer in contact with air would be oxidized to form and an ultra-thin layer an oxide layer with a thickness of only 3 nm on the top. According to our calculation, the oxidation only shifts the center wavelength with only 2 nm and reduces the peak value in transmittance only 0.4%. Figure 5 presents the transmittance spectra of the designed and deposited filter. The transmittance peak of the deposited multilayered is shifted to 946 nm from the designated wavelength of 950 nm and the transmittance maximum is reduced to 74%. Figure 6 plots the transmittance versus wavelength and AOI. The transmittance peak in the p-polarized spectra is slightly shifted from 946 nm to 937 nm as the AOI increases from 0° to 60° , and the passband is low angle-dependent. The peak value of the p-polarized transmittance decays from 74% at AOI = 0° to 69% at AOI = 60° at a wavelength of 948 nm. The transmittance peak in the s-polarized spectra is slightly shifted from 948 nm to 930 nm as the AOI is increased from 0° to 50° , and the pass band is almost angle-independent. The peak s-polarized transmittance decays from 74% at AOI = 0° to 66% at AOI = 50° at a wavelength of 948 nm.

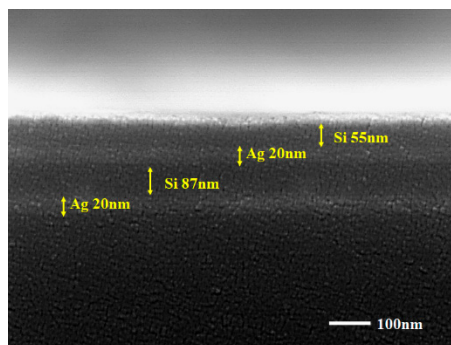


Figure 4. Scanning electron microscope (SEM) image of cross-section of fabricated sample; thicknesses of layers $N_i/D_1M_2D_3M_4/N_{sub} = \text{air/a-Si (55 nm)/Ag (20 nm)/a-Si (87 nm)/Ag (20 nm)/glass}$.

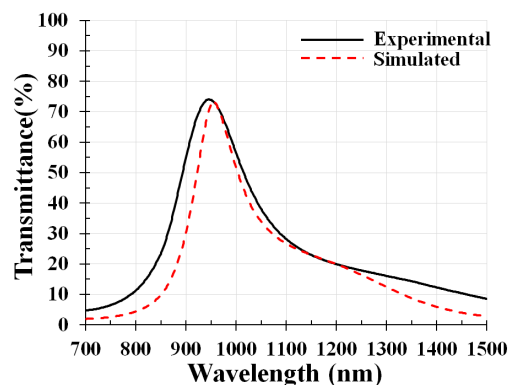


Figure 5. Transmittance spectra of designed and deposited experimental multilayers, air/a-Si/Ag/a-Si/Ag/glass.

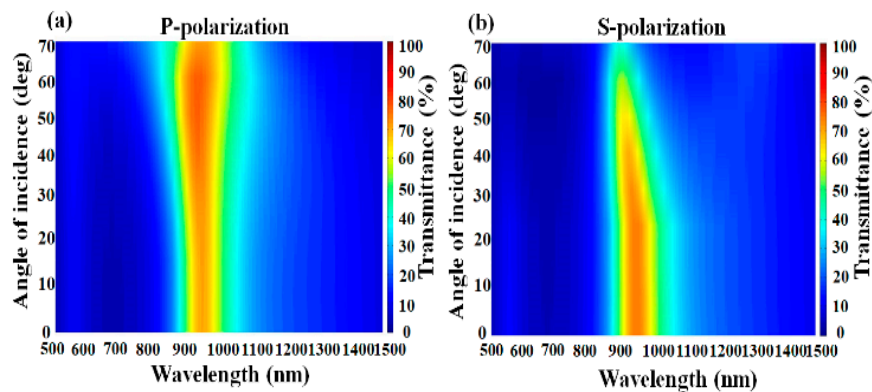


Figure 6. Measurement of (a) p-polarized and (b) s-polarized transmittances of deposited multilayer as functions of wavelength and angle of incidence.

4. Conclusions

In this work, silver and silicon are used in the optical coating of an angle-insensitive filter. Based on the characteristic of a modified Fabry–Perot filter on NAD, five-layered and four-layered narrow bandpass filters in the infrared range are developed. A compact four-layered structure exhibits a single passband with FWHM = 117 nm over wavelengths from 700 nm to 1500 nm. The relative wavelength shift $\Delta\lambda/\lambda_0$ is only 10 nm as AOI increases from 0° to 60° . The peak transmittance exceeds 74% and decays to 68% as AOI increases from 0° to 60° . The proposed method offers a promising avenue toward the realization of any metal with a low index of refraction and a dielectric with a high index of refraction. Such wide-angle filters can be applied in many fields, including image recognition, and in light-emissive diodes.

Author Contributions: Conceptualization, Y.-J.J.; Methodology, Y.-J.J. and M.-J.L.; Validation, Y.-J.J. and M.-J.L.; Formal Analysis, Y.-J.J.; Investigation, Y.-J.J. and M.-J.L.; Resources, Y.-J.J.; Data Curation, M.-J.L.; Writing-Original Draft Preparation, Y.-J.J. and M.-J.L.; Writing-Review & Editing, Y.-J.J. and M.-J.L.; Supervision, Y.-J.J.; Project Administration, Y.-J.J.; Funding Acquisition, Y.-J.J.

Funding: This research received no external funding.

Acknowledgments: The authors would like to thank Zheng-Xing Li, Ming-Zheng Li, Zhi-Heng Yu, Yu-Sin Chang, Hsiang-Yu Yang, and Tzu-Huan Hsu for their assistance during fabrication of thin films.

Conflicts of Interest: The authors declare no conflict of interest.

Appendix A

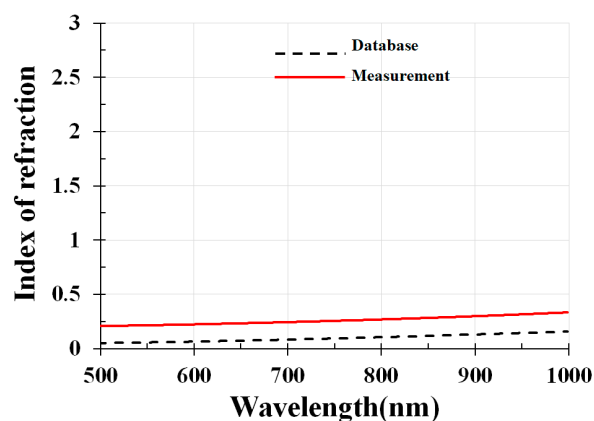


Figure A1. The indexes of refraction of Ag versus wavelength from measurement and database.

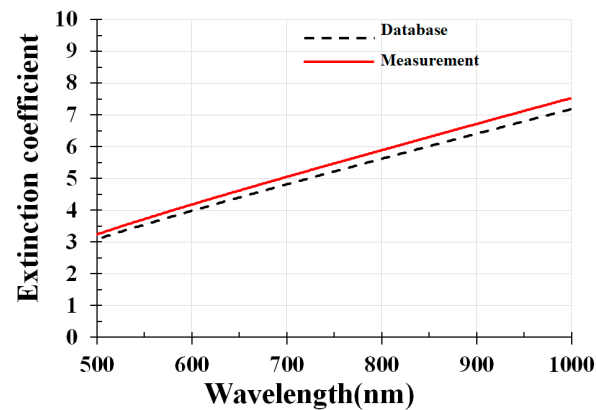


Figure A2. The extinction coefficients of Ag versus wavelength from measurement and database.

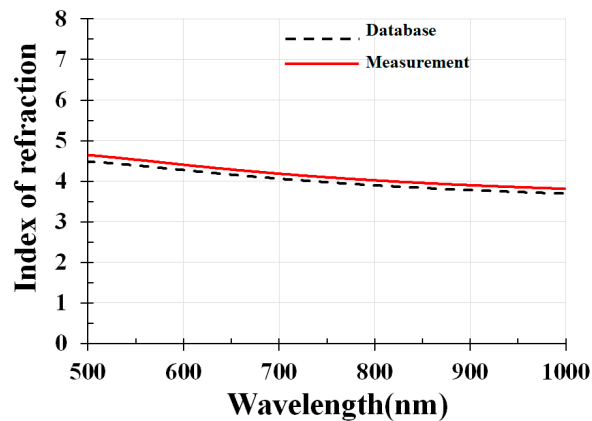


Figure A3. The indexes of refraction of a-Si versus wavelength from measurement and database.

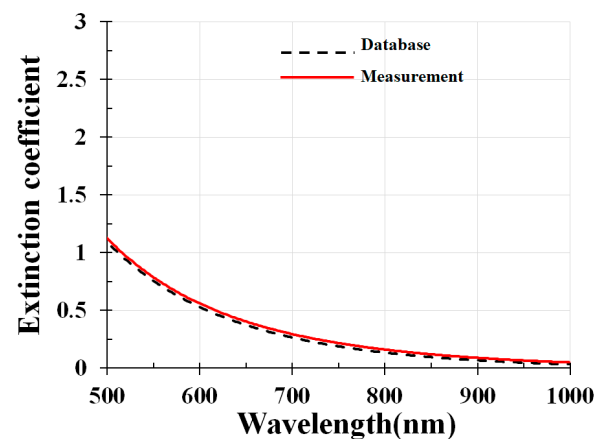


Figure A4. The extinction coefficients of a-Si versus wavelength from measurement and database.

References

1. Koo, H.; Chen, M.; Pan, P. LCD-based color filter films fabricated by a pigment-based colorant photo resist inks and printing technology. *Thin Solid Films* **2006**, *515*, 896–901. [[CrossRef](#)]
2. Ko, F.-J.; Shieh, H.-P.D. High-efficiency micro-optical color filter for liquid-crystal projection system applications. *Appl. Opt.* **2000**, *39*, 1159–1163. [[CrossRef](#)] [[PubMed](#)]

3. Chung, D.; Shin, C.; Song, B.; Jung, M.; Yun, Y.; Nam, S.H.; Noh, C.; Kim, J.; Lee, S. Color filters for reflective display with wide viewing angle and high reflectivity based on metal dielectric multilayer. *Appl. Phys. Lett.* **2012**, *101*, 221120. [[CrossRef](#)]
4. Kanamori, Y.; Shimono, M.; Hane, K. Fabrication of transmission color filters using silicon subwavelength gratings on quartz substrates. *IEEE Photonics Technol. Lett.* **2006**, *18*, 2126–2128. [[CrossRef](#)]
5. Park, J.-G.; Kim, S.-H.; Magkiriadou, S.; Choi, T.M.; Kim, Y.-S.; Manoharan, V.N. Full-spectrum photonic pigments with non-iridescent structural colors through colloidal assembly. *Angew. Chem. Int. Ed.* **2014**, *53*, 2899–2903. [[CrossRef](#)] [[PubMed](#)]
6. Macleod, H. *Thin Film Optical Filters*, 3rd ed.; Institute of Physics Publishing: Bristol, UK, 2001.
7. Yang, C.; Shen, W.; Zhang, Y.; Li, K.; Fang, X.; Zhang, X.; Liu, X. Compact multilayer film structure for angle insensitive color filtering. *Sci. Rep.* **2015**, *5*, 9285. [[CrossRef](#)] [[PubMed](#)]
8. Si, G.; Zhao, Y.; Lv, J.; Lu, M.; Wang, F.; Liu, H.; Xiang, N.; Huang, T.J.; Danner, A.J.; Teng, J.; et al. Reflective plasmonic color filters based on lithographically patterned silver nanorod arrays. *Nanoscale* **2013**, *5*, 6243–6248. [[CrossRef](#)] [[PubMed](#)]
9. Ai, B.; Yu, Y.; Mohwald, H.; Zhang, G. Color displays: Responsive monochromatic color display based on nanovolcano arrays. *Adv. Opt. Mater.* **2013**, *1*, 724–731. [[CrossRef](#)]
10. Lin, L.; Roberts, A. Angle-robust resonances in crossshaped aperture arrays. *Appl. Phys. Lett.* **2010**, *97*, 061109. [[CrossRef](#)]
11. Xu, T.; Wu, Y.-K.; Luo, X.; Guo, L.J. Plasmonic nanoresonators for high-resolution colour filtering and spectral imaging. *Nat. Commun.* **2010**, *59*. [[CrossRef](#)] [[PubMed](#)]
12. Jen, Y.-J.; Lee, C.-C.; Lu, K.-H.; Jheng, C.-Y.; Chen, Y.-J. Fabry-Perot based metal-dielectric multilayered filters and metamaterials. *Opt. Exp.* **2015**, *23*, 33008–33017. [[CrossRef](#)] [[PubMed](#)]
13. Morita, M.; Ohmi, T.; Hasegawa, E.; Kawakami, M.; Ohwada, M. Growth of native oxide on a silicon surface. *J. Appl. Phys.* **1990**, *68*, 1272–1281. [[CrossRef](#)]
14. Ryckman, J.D.; Reed, R.A.; Weller, R.A.; Fleetwood, D.M.; Weissa, S.M. Enhanced room temperature oxidation in silicon and porous silicon under 10 keV X-ray irradiation. *J. Appl. Phys.* **2010**, *108*, 113528. [[CrossRef](#)]



© 2018 by the authors. Licensee MDPI, Basel, Switzerland. This article is an open access article distributed under the terms and conditions of the Creative Commons Attribution (CC BY) license (<http://creativecommons.org/licenses/by/4.0/>).